Int. J. Solids Structures, 1974, Vol. 10, pp. 903–917. Pergamon Press. Printed in Gt. Britain.

COMBINED PLASTIC WAVES IN A THIN-WALLED TUBE

HAN-CHIN WU† and HSUAN-CHI LIN‡

Department of Mechanics and Hydraulics, University of Iowa, Iowa City, Iowa 52242, U.S.A.

(*Received* 22 *August* 1973; *revised* 17 *December* 1973)

Abstract—A theory of plasticity without a yield surface is applied to obtain the simple wave solution of a thin-walled tube subject to the combined step loading. Four wave speeds are obtained in this analysis; all speeds involve the coupling of the longitudinal and the torsional motions as well as the loading and the unloading behaviors. Several numerical examples of our theoretical analysis and their comparisons with the experimental data and with the existing theory are also presented. The constant state region between slow and fast waves is not apparent in the present analysis. This is in good agreement with the experiment. Moreover, the predicted final state of shear strain is higher than the experimental, but less than Lipkin and Clifton's result.

1. INTRODUCTION

We consider in this paper a long slender thin-walled cylindrical tube subject to a suddenly applied combined longitudinal and torsional motion (or stress) at one end. Ignoring the radial motion, the only non-zero velocities of an element on the tube are the longitudinal velocity u and the circumferential velocity v. Similarly, the only non-zero stresses are the longitudinal stress σ and the torsional stress τ.

The above problem has acquired the attention of researchers only rather recently in both the theoretical and the experimental works [1–9]. Most of the published works are, however, to the present investigators' knowledge, based on the flow theory of plasticity and on the assumption of the strain-rate independency of the material.

The first attempt in the theoretical study of this problem was due to Clifton[1]. In his work, Clifton considered an isotropic work-hardening material. The tube was of semi-infinite length and the loads $\sigma(0, t)$ and $\tau(0, t)$ applied at the end of the tube were step functions of time. He obtained a simple wave solution and observed the existence of two wave speeds, namely, the fast wave speed C_f and the slow wave speed C_{sl}. These two wave speeds were related to the elastic dilitational wave speed $C_D = \sqrt{E/\rho}$ and elastic shear wave speed $C_S = \sqrt{\mu/\rho}$ by the inequalities $0 \leq C_{sl} \leq C_S \leq C_F \leq C_D$, where ρ is the density; E and μ are, respectively, the elastic and shear modulus. For each wave speed, the longitudinal and torsional stresses were coupled and propagated along the tube.

The same problem was generalized by Lipkin and Clifton[2] to include materials obeying the kinematic work-hardening law. Goel and Malvern[3] proposed a method accounting for the combined effects of the isotropic and kinematic hardening law. Ting[4] obtained

† Assistant Professor.
‡ Research Assistant.

solutions for all possible combinations of discontinuous loadings at $t = 0$ and for all possible variations of loads thereafter. He also obtained an explicit simple wave solution for linear work-hardening materials[5]. Fukuoka[6] and Janssen *et al.*[7], interpreting waves as propagating singular surfaces, investigated the cases where the rear and the front of the surface were in the same or in different states.

The experimental works done to date which are related to our problem are those due to Lipkin and Clifton[2, 8]. These experimental results show the nature of two distinct types of wave both of which involve coupled longitudinal and torsional motion, and the main features of these waves are in qualitative agreement with theoretical prediction discussed above. There are, however, systematic qualitative and quantitative discrepancies between the predicted and the observed responses. The constant strains in the region between the fast and slow wave, as predicted by the theory, were not observed in the experiments. In addition, the predicted final state of shear strain was considerably greater than the measured value. Lipkin and Clifton[8] indicated that the discrepancies were probably due to the inadequate assumption of the strain-hardening law. Since the loading paths that occurred in the experiments were quite complicated, a different assumption of the strain-hardening law would likely alter considerably the predicted results. Some discrepancies were attributed to the negligence of the strain-rate dependency of materials. A theoretical work related to the present problem was presented by Cristescu[9] for a class of rate-sensitive material. A main conclusion was that the coupling of the shearing wave and longitudinal wave existed in all the four waves obtained in the analysis. No comparisons with the experimental results were presented in the paper.

From the foregoing review, it is clear that the existing theoretical solution of the combined plastic wave problem is far from being satisfactory. The systematic discrepancies, both qualitative and quantitative, between the predicted and the observed results are believed by the present investigators to have their roots in the theory of plasticity adopted in the theoretical analysis. In the existing analysis, the flow theory of plasticity was employed. This theory inherited the uncertainties from the definition of a yield surface and the proposition of a strain-hardening law.†

In this work, the endochronic theory of plasticity[10], which does not define a concept of yield surface and therefore removes the uncertainties associated with this concept, will be applied to obtain the solution of the problem described above. This is the dynamic version of the two quasi-static problems investigated by Valanis[10], i.e. hardening in tension due to torsional prestrain, and the behavior in tension with presence of shear stress due to torsion. The endochronic theory has already been shown to have advantages in handling problems of this kind. In following sections, we shall formulate the problem first, then the constitutive equations based on the assumption of plastic incompressibility of material will be derived. In Section 4, simple wave solutions will be obtained by use of a one-parameter constant conformal invariant transformation with similarity variable $\xi = x/t$. Several numerical examples will be presented in Section 5, and finally, comparisons of our theoretical results with the experimental data and the existing theory will be made.

2. THE FUNDAMENTAL EQUATIONS

In the formulation of the problem, due to the small wall thickness and the axial symmetry, there are only two independent variables; namely, the time t, and the distance x along the

† For more critical discussions, see Ref.[10].

tube axis. Furthermore, if we neglect the radial motion, the only non-zero stress components are the axial stress σ and the shear stress τ. The conservation of linear momentum then gives us

$$\sigma_x = \rho u_t \tag{1a}$$

$$\tau_x = \rho v_t \tag{1b}$$

where ρ is the density; u and v are the longitudinal and circumferential particle velocities, respectively. The body forces are neglected in the analysis. The subscripts x and t denote the partial differentiation with respect to the corresponding variable. Similarly, for small strains, the only non-zero strain components are the longitudinal strain ε and the torsional strain η. Thus from compatibility conditions we have

$$\varepsilon_t = u_x \tag{2a}$$

$$\eta_t = \tfrac{1}{2} v_x . \tag{2b}$$

Equations (1) and (2) together form the fundamental equations of our problem.

3. THE CONSTITUTIVE EQUATIONS

The constitutive equations for isotropic materials under isothermal and small strain conditions are given by Valanis[10], with the assumption of elastic hydrostatic response, as follows:

$$s_{ij} = 2\int_0^z \mu(z - z')\frac{\partial e_{ij}}{\partial z'}\,\mathrm{d}z' \tag{3a}\dagger$$

$$\sigma_{kk} = 3K\varepsilon_{kk} \tag{3b}$$

where s_{ij} and e_{ij} are deviatoric stress and strain tensors; $\mu(z)$ and K are heredity function and bulk mudulus, respectively. The symbol z denotes a positive monotonically increasing time scale with respect to a time measure ζ such that

$$\mathrm{d}\zeta^2 = P_{ijkl}\,\mathrm{d}\varepsilon_{ij}\,\mathrm{d}\varepsilon_{kl}$$

where P_{ijkl} is a material tensor, which is positive definite and which for isotropic materials has the form

$$P_{ijkl} = K_1\delta_{ij}\delta_{kl} + \tfrac{1}{2}K_2(\delta_{ik}\delta_{jl} + \delta_{il}\delta_{jk})$$

such that $K_1 + \dfrac{K_2}{3} \geq 0$, $K_2 \geq 0$; K_1 and K_2 may not both be zero. We then have

$$\mathrm{d}\zeta^2 = K_1\,\mathrm{d}\varepsilon_{kk}\,\mathrm{d}\varepsilon_{ll} + K_2\,\mathrm{d}\varepsilon_{ij}\,\mathrm{d}\varepsilon_{ij} \tag{4}$$

using the above relations. Now, if we let

$$\mu(z) = \mu_0\,\mathrm{e}^{-\alpha z}$$

μ_0 and α being material constants, and substitute the above relation into (3a) we get

$$s_{ij} = 2\mu_0\int_0^z \mathrm{e}^{-\alpha(z-z')}\frac{\partial \mathrm{e}_{ij}}{\partial z'}\,\mathrm{d}z'$$

† Equation (3) has been shown to be adequate in predicting metallic responses, such as cross-hardening, loading and unloading loops, behavior in tension in the presence of a shearing stress, cyclic hardening as well as cyclic softening[10, 15].

or equivalently we may write, for the above equation, the following

$$\frac{\mathrm{d}s}{\mathrm{d}z} + \alpha s = 2\mu_0 \frac{\mathrm{d}e}{\mathrm{d}z}.$$

Moreover, if we introduce [10]

$$\mathrm{d}z = \frac{\mathrm{d}\zeta}{1 + \beta\zeta}$$

then the above equation becomes

$$2\mu_0 \frac{\mathrm{d}e}{\mathrm{d}\zeta} = \frac{\alpha s}{1 + \beta\zeta} + \frac{\mathrm{d}s}{\mathrm{d}\zeta}. \tag{3c}$$

Thus, Equations (3b) and (3c) are the constitutive equations subject to the intrinsic time measure (4).

For the combined tension and torsion of a thin-walled tube,

$$\boldsymbol{\sigma} = \begin{pmatrix} \sigma & \tau & 0 \\ \tau & 0 & 0 \\ 0 & 0 & 0 \end{pmatrix}; \qquad \boldsymbol{s} = \begin{pmatrix} \frac{2}{3}\sigma & \tau & 0 \\ \tau & -\frac{1}{3}\sigma & 0 \\ 0 & 0 & -\frac{1}{3}\sigma \end{pmatrix}$$

and

$$\boldsymbol{\varepsilon} = \begin{pmatrix} \varepsilon & \eta & 0 \\ \eta & \varepsilon_2 & 0 \\ 0 & 0 & \varepsilon_2 \end{pmatrix}; \qquad \boldsymbol{e} = \begin{pmatrix} \frac{2}{3}(\varepsilon - \varepsilon_2) & \eta & 0 \\ \eta & -\frac{1}{3}(\varepsilon - \varepsilon_2) & 0 \\ 0 & 0 & -\frac{1}{3}(\varepsilon - \varepsilon_2) \end{pmatrix}.$$

We note that ε_2 has been considered for the time being and will be made equal to zero later in this paper. For the above stress and strain states, equation (3b) becomes

$$\mathrm{d}\sigma = 3K(\mathrm{d}\varepsilon + 2\mathrm{d}\varepsilon_2)$$

and for $i, j = 1$, equation (3c) yields

$$2\mu_0(\mathrm{d}\varepsilon - \mathrm{d}\varepsilon_2) = \frac{\alpha\sigma\,\mathrm{d}\zeta}{1 + \beta\zeta} + \mathrm{d}\sigma.$$

Eliminating $\mathrm{d}\varepsilon_2$ from the above two equations, we then obtain

$$\mathrm{d}\varepsilon = \frac{\alpha}{3\mu_0} \frac{\sigma\,\mathrm{d}\zeta}{1 + \beta\zeta} + \left(\frac{1}{3\mu_0} + \frac{1}{9K}\right)\mathrm{d}\sigma.$$

Since the initial slope E_0 of the longitudinal stress–strain curve is related to μ_0 and K by

$$E_0 = \frac{3\mu_0}{1 + \dfrac{\mu_0}{3K}}$$

the above equation may be simplified to read

$$E_0\,\mathrm{d}\varepsilon = \frac{E_0\alpha}{3\mu_0} \frac{\sigma\,\mathrm{d}\zeta}{1 + \beta\zeta} + \mathrm{d}\sigma. \tag{5a}$$

Similarly, we obtain from Equation (3c)

$$2\mu_0 \, d\eta = \frac{\alpha\tau \, d\zeta}{1 + \beta\zeta} + d\tau. \tag{5b}$$

Comparing equation (5) with the corresponding equations derived under the assumption of constant Poisson's ratio, we find that the only difference is in the factor of $E_0/3\mu_0$ on the right-hand side of equation (5a). Furthermore, if we neglect the lateral inertia effect, i.e. $\varepsilon_2 = 0$ in the small strain tensor, then Equation (4) reduces to

$$d\zeta^2 = k_1^2 (d\varepsilon)^2 + k_2^2 (d\eta)^2 \tag{6}$$

which is the same as the result from the assumption of constant Poisson's ratio. Thus, equations (5a and 5b), together with equation (6) form the constitutive equations for the material considered in our problem.

To determine the material parameters in the constitutive equations, the same procedures as described in Ref.[10] may be followed. For the uniaxial tension without shear prestrain, equation (5a) reduces to

$$\sigma = \frac{E_0}{\beta_1 n} (1 + \beta_1 \varepsilon) [1 - (1 + \beta_1 \varepsilon)^{-n}]$$

where

$$n = 1 + \frac{\alpha'}{\beta}$$

$$\alpha' = \frac{E_0}{3\mu_0} \alpha = a\alpha; \qquad a = \frac{E_0}{3\mu_0}$$

$$\beta_1 = k_1 \beta.$$

Let

$$\alpha_1 = k_1 \alpha'$$

then

$$n = 1 + \frac{\alpha_1}{\beta_1}. \tag{7a}$$

As ε increases, σ tends asymptotically to the linear expression

$$\sigma = \frac{E_0}{\beta_1 n} (1 + \beta_1 \varepsilon).$$

If E_t is the slope of the asymptotic straight line, then

$$n = \frac{E_0}{E_t}. \tag{7b}$$

Furthermore, if σ_0 denotes the intercept of the asymptotic straight line with the stress axis, then

$$\beta_1 = \frac{E_t}{\sigma_0}. \tag{7c}$$

Thus, the three material parameters n, β_1, α_1 can be determined from the uniaxial tension test through the three relations (7a), (7b) and (7c).

Similarly, for pure shear test, from equation (5b) we have

$$\tau = \frac{2\mu_0}{\beta_2 m}(1+\beta_2\eta)\,[1-(1+\beta_2\eta)^{-m}]$$

where

$$m = 1 + \frac{\alpha_2}{\beta_2}; \qquad \alpha_2 = k_2\alpha; \qquad \beta_2 = k_2\beta \tag{7d}$$

$$m = \frac{\mu_0}{\mu_t} \tag{7e}$$

$$\beta_2 = \frac{2\mu_0}{\tau_0} \tag{7f}$$

and μ_t and τ_0 are respectively the slope of the asymptotic straight line and its intercept with the stress axis of the shear stress–strain curve. Therefore, the other three material parameters m, β_2, α_2 can also be determined by using equations (7d), (7e) and (7f). Finally from equations (7a) and (7d), we obtain the following relation

$$\frac{m-1}{n-1} = \frac{3\mu_0}{E_0} \tag{7g}$$

which is the consistency relation to be satisfied by the assumption of material plastic incompressibility.

4. THE SIMPLE WAVE SOLUTIONS

For later convenience, let us summarize the basic equations we have derived in the previous two sections. The equations of motion and the compatibility conditions are:

$$\sigma_x = \rho u_t \tag{8a}$$

$$\tau_x = \rho v_t \tag{8b}$$

$$\varepsilon_t = u_x \tag{8c}$$

$$\eta_t = \tfrac{1}{2} v_x . \tag{8d}$$

The constitutive equations are:

$$E_0\,\varepsilon_t = \frac{\alpha'\sigma}{1+\beta\zeta}\,\zeta_t + \sigma_t \tag{8e}$$

$$2\mu_0\,\eta_t = \frac{\alpha\tau}{1+\beta\zeta}\,\zeta_t + \tau_t \tag{8f}$$

$$(\zeta_t)^2 = (k_1\varepsilon_t)^2 + (k_2\eta_t)^2. \tag{8g}$$

Following the general procedures of similarity transformation, let us consider a one-parameter group transformation applying to the above set of first order partial differential equations with independent variables x and t. For the constant conformal invariant transformation, we may choose $\xi = x/t$ as the similarity variable and all dependent variables themselves as invariants. This procedure would lead to a simple wave solution in which the

solution is constant along a straight characteristic line $dx/dt = \text{constant}$. Performing the substitution of this new variable into the above set of p. d. e., equations (8a) to (8d) become the following ordinary differential equations with only one independent variable ξ.

$$\sigma' = -\rho\xi u' \tag{9a}$$

$$\tau' = -\rho\xi v' \tag{9b}$$

$$\varepsilon' = \frac{1}{\rho\xi^2}\sigma' \tag{9c}$$

$$\eta' = \frac{1}{2\rho\xi^2}\tau' \tag{9d}$$

where equations (9a) and (9b) have been used in deriving equations (9c) and (9d) and the prime stands for the differentiation with respect to ξ. Substituting equation (8g) into (8e) and (8f), carrying out the same similarity transformation and making use of the above relations, we get the following two homogeneous first order o.d.e.,

$$\left\{(\rho\xi^2 - E_0)^2 - \left(\frac{\alpha_1\sigma}{1+\beta\zeta}\right)^2\right\}(\sigma')^2 - \left(\frac{a}{2}\frac{\alpha_2\sigma}{1+\beta\zeta}\right)^2(\tau')^2 = 0 \tag{9e}$$

$$\left(\frac{1}{a}\frac{\alpha_1\tau}{1+\beta\zeta}\right)^2(\sigma')^2 - \left\{(\rho\xi^2 - \mu_0)^2 - \left(\frac{1}{2}\frac{\alpha_2\tau}{1+\beta\zeta}\right)^2\right\}(\tau')^2 = 0. \tag{9f}$$

Equations (9e) and (9f) have a non-trivial solution if the determinant of the coefficient matrix vanishes, i.e.

$$\left\{(\rho\xi^2 - E_0)^2 - \left(\frac{\alpha_1\sigma}{1+\beta\zeta}\right)^2\right\}\left\{(\rho\xi^2 - \mu_0)^2 - \left(\frac{1}{2}\frac{\alpha_2\tau}{1+\beta\zeta}\right)^2\right\} - \left(\frac{a}{2}\frac{\alpha_2\sigma}{1+\beta\zeta}\right)^2\left(\frac{1}{a}\frac{\alpha_1\tau}{1+\beta\zeta}\right)^2 = 0$$

or

$$\begin{aligned}(\rho\xi^2)^4 &- 2(E_0+\mu_0)(\rho\xi^2)^3 \\ &+ \left\{(E_0+\mu_0)^2 + 2E_0\mu_0 - \left(\frac{\alpha_1\sigma}{1+\beta\zeta}\right)^2 - \left(\frac{1}{2}\frac{\alpha_2\tau}{1+\beta\zeta}\right)^2\right\}(\rho\xi^2)^2 \\ &+ \left\{2\mu_0\left(\frac{\alpha_1\sigma}{1+\beta\zeta}\right)^2 + 2E_0\left(\frac{1}{2}\frac{\alpha_2\tau}{1+\beta\zeta}\right)^2 - 2E_0\mu_0(E_0+\mu_0)\right\}(\rho\xi^2) \\ &+ \left\{E_0^2\mu_0^2 - \left(\frac{\mu_0\alpha_1\sigma}{1+\beta\zeta}\right)^2 - \left(\frac{1}{2}\frac{E_0\alpha_2\tau}{1+\beta\zeta}\right)^2\right\} = 0.\end{aligned} \tag{10}$$

This is the characteristic equation for equations (9e) and (9f). The characteristic velocities are the roots of the above equation. There are four roots in this quartic equation. Although the character of these four roots are not obvious, the numerical results indicate the following inequalities

$$c_1 \geq c_D \geq c_2 \geq c_3 \geq c_S \geq c_4 \tag{11}\dagger$$

† C_D and C_S correspond directly to the initial slopes of the stress–strain curves. Since hysteresis loops exist in the loading–unloading cycles, wave speed may exceed the conventional elastic wave speed.

where C_1, C_2, C_3 and C_4 are the four roots of the characteristic equation. The root C_4 leads to the "slow wave", whereas C_2 and C_3 correspond to the "fast waves" in Clifton's definition. For the initial-boundary value problems considered in this paper, the numerical results show that all roots are real in the fast wave region; while C_2 and C_3 may become complex in the slow wave region. However, if the initial condition is such that the stress point in the stress-space is located within the slow wave region mentioned above, the wave speeds C_2 and C_3 are then real. This is so because our characteristic values depend not only on the current stress but also on the deformation history. In view of (11), it is clear that the longitudinal and torsional motions are coupled involving both loading and unloading behaviors.

On the other hand, equations (9e) and (9f) lead to the following relations:

$$\frac{d\tau}{d\sigma} = \frac{\sqrt{(\rho\xi^2 - E_0)^2 - \left(\frac{\alpha_1\sigma}{1+\beta\zeta}\right)^2}}{\frac{a}{2}\frac{\alpha_2\sigma}{1+\beta\zeta}} \tag{12a}$$

$$\frac{d\tau}{d\sigma} = \frac{\frac{1}{a}\frac{\alpha_1\tau}{1+\beta\zeta}}{\sqrt{(\rho\xi^2 - \mu_0)^2 - \left(\frac{1}{2}\frac{\alpha_2\tau}{1+\beta\zeta}\right)^2}}. \tag{12b}$$

In view of equation (10) we may also express (12a) or (12b) in terms of the wave speed as follows

$$\frac{d\tau}{d\sigma} = \left(\frac{\rho\xi^2 - E_0}{\rho\xi^2 - \mu_0}\right)\left(\frac{\tau}{a\sigma}\right). \tag{12c}$$

Equations (12a), (12b) or (12c) represent the stress trajectory which is the path in the stress-space at a cross section of the tube following the passage of the simple waves. From equation (12c), it is obvious that the slope of the stress trajectory is negative for the "fast" wave and positive for the slow" wave if both σ and τ are positive. This determines the directions of the stress paths.

The stress trajectory and the corresponding wave speeds are not determined *a priori*, since they both involve the value of the current stress state as well as the deformation history. When the numerical integration scheme is applied, one can solve equations (10) and (12c) at each step. Once the wave speeds and the changes of stress state are found, the corresponding particle velocities u and v and the changes of ε and η can be obtained through equations (9a) to (9d). As a consequence of equations (9a) and (9b) we may have the following relation

$$\frac{du}{dv} = \frac{d\sigma}{d\tau}. \tag{13a}$$

Similarly, from equations (9c) and (9d) we obtain

$$\frac{d\varepsilon}{2d\eta} = \frac{d\sigma}{d\tau}. \tag{13b}$$

That is, the direction of the total strain rate vector coincides with that of the stress rate vector. This is a result which was first obtained by Clifton using a different approach[1].

5. NUMERICAL RESULTS AND DISCUSSION

In order to compare the computed results with the available experimental data, let us make use of the experimental stress–strain curve for annealed 3003 aluminum which appeared in Ref.[8]. According to the procedures described in Section 3, the material parameters n, β_1, α_1 can be obtained from this curve. The resulting stress–strain curve together with the experimental stress–strain curve are shown in Fig. 1. As far as the experimental shear stress–strain curve is concerned, it is, unfortunately, not available in the literature. It was suggested by Clifton† that the concept of an "equivalent stress–strain curve" based on the von Mises yield condition and isotropic hardening may be utilized to obtain the corresponding shear stress–strain curve for the material under consideration. If the above procedure is carried out, we may obtain the other material parameters m, β_2, and α_2. Thus, all material parameters may be found and their values are presented in Fig. 1.

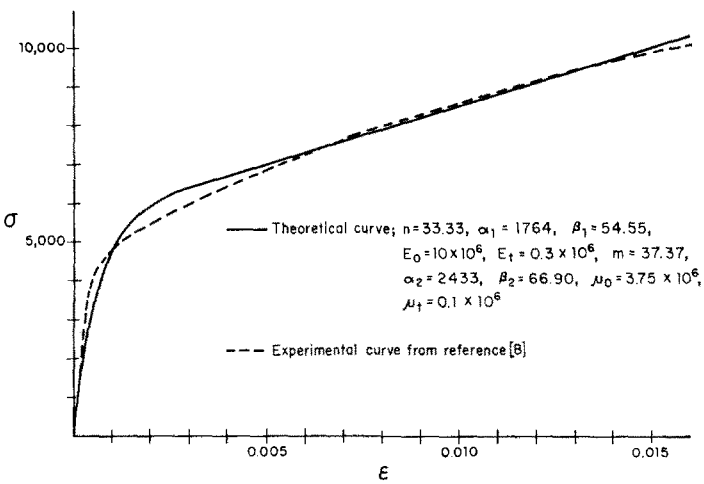

Fig. 1. Stress–strain curves for annealed 3003 aluminum.

A fourth order Runge–Kutta method has been applied to perform the numerical integration. Based on the values of all material parameters as determined above, the stress paths for the simple waves are first constructed as shown in Fig. 2. It is seen that the shape of the fast simple waves in this computational result is different from that reported in Refs.[1] and[3], in which the von Mises yield condition is employed and isotropic, kinematic or combined work-hardening assumptions are made. In Refs.[1] and [3] the paths of fast simple waves are seen to be directly related to the shapes of the subsequent yield surface, which are elliptical because of the assumptions made in those papers. Experimental results by Ivey[11] and Phillips and Tang[12] show that the shape of the subsequent yield surface is quite complicated and depends greatly upon the loading history. In view of the above argument, it seems that our shape of fast simple waves may represent certain "yield surface" in that loading history. It may also notice that in Fig. 2, the paths of slow simple waves far

† Private communication.

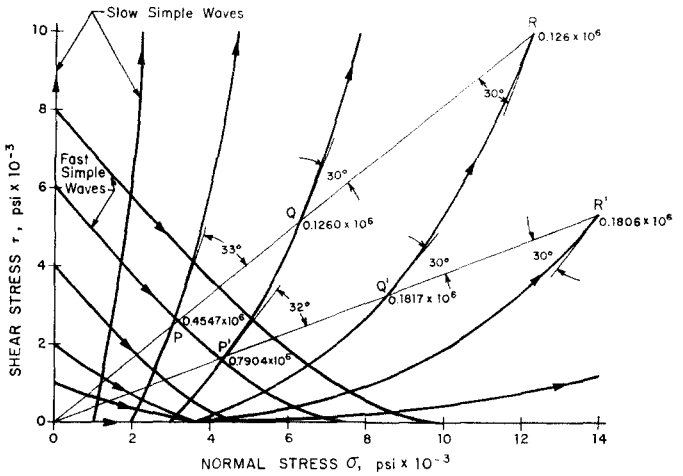

Fig. 2. Stress paths for simple waves.

enough from the origin intersect the radial line τ/σ = constant at the same angle with approximately the same characteristic wave speeds. This result agrees with that of Ting[5] in which all stress paths are "similar" in linearly work-hardening material. This agreement is due to the fact that in our stress–strain curve, for sufficiently large strain, the relationship between stress and strain is almost linear as seen from Fig. 1.

A solution which satisfies the initial and boundary conditions is obtained in the same way as in the paper by Clifton[1]†. First, a fast simple wave solution is computed for which the stress trajectory passes through the initial state of prestress. Then, slow simple wave solutions are computed starting at various points along the fast simple wave stress trajectory until that point is found for which the slow simple wave particle velocity trajectory (or whatever the boundary conditions are prescribed) passes through the point (u_0, v_0) corresponding to the constant velocity at the boundary.

The results of three initial and boundary value problems as described in[8] will be reported here. Comparisons of strain–time profiles (during loading only) for three different impact velocities with different initial torques are presented in Figs. 3, 5 and 9, and comparisons of the associated strain trajectories are presented in Figs. 4, 6 and 10. The stress and particle velocity trajectories corresponding to the present theory and that of Lipkin and Clifton[8] for the case of Fig. 5 are also shown in Figs. 7 and 8. The prescribed prestress and velocity boundary conditions are given in each figure. In the strain trajectory figures, the final stress states (normal stress σ_0 and shear stress τ_0) at the boundary following the slow wave from results of experiment, the analysis of Lipkin and Clifton and the present theory are also given for comparison.

The comparisons of the strain–time profiles show several characteristic differences among present theory, Lipkin and Clifton's analysis and the experiment[8]. First of all, the constant state region between slow and fast waves as appeared in Lipkin and Clifton's analysis is not apparent in the present theory although there must exist a very small constant state region there. This is in good agreement with the experiment. Secondly, the end of the fast

† It can be shown that, for our non-linear equations, the lines x/t = constant along which simple waves and constant state regions are pieced together are characteristics so that discontinuous derivatives are admissible across such lines.

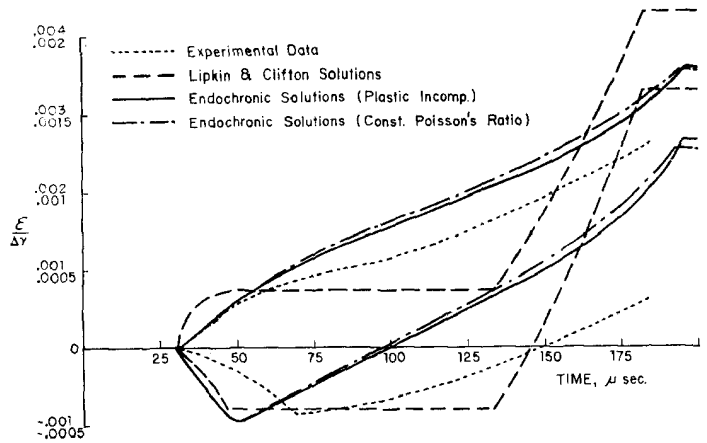

Fig. 3. Comparison of computed and experimental strain–time profiles at $x = 6{\cdot}25$ in. ($\tau_s =$ 3220 psi, $u_0 = 260$ ips, $v_0 = 17$ ips).

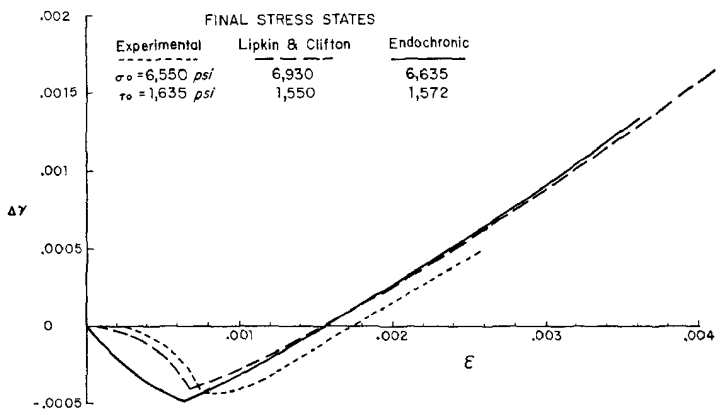

Fig. 4. Comparison of computed and experimental strain trajectories at $x = 6{\cdot}25$ in. ($\tau_s = 3220$ psi, $u_0 = 260$ ips, $v_0 = 17$ ips).

wave, as distinguished by the sharp change in slope of the shear strain–time profile, arrives consistently later in experiment than predicted by both theories. This delay as indicated in Ref.[8] may be due to the finite rise time of the actual velocities at the boundary. Moreover, the shear strain–time profile in the present theory approaches a value which is higher than the experimental but less than Lipkin and Clifton's result; whereas the values of longitudinal strain are of comparable magnitude among theories and the experiment. The qualitative and quantitative differences between the present theory and the experiment are less than the differences between Lipkin and Clifton's analysis and the experiment for smaller impact velocities whereas the reverse is true for higher impact velocities. This qualitative difference between the present theory and the experiment for higher impact velocity such as the one shown in Fig. 9 is probably due to the character of our stress–strain curve. For $\varepsilon > 0{\cdot}004$, this curve tends to an asymptotic straight line and the shock wave would occur if the impact velocity is greater than certain value. Finally, the present theory predicts constant strain plateaus after slow simple waves. This is in agreement with the results of Karman–Duwez[13], Wood–Phillips[14], as well as the well-known experimental results

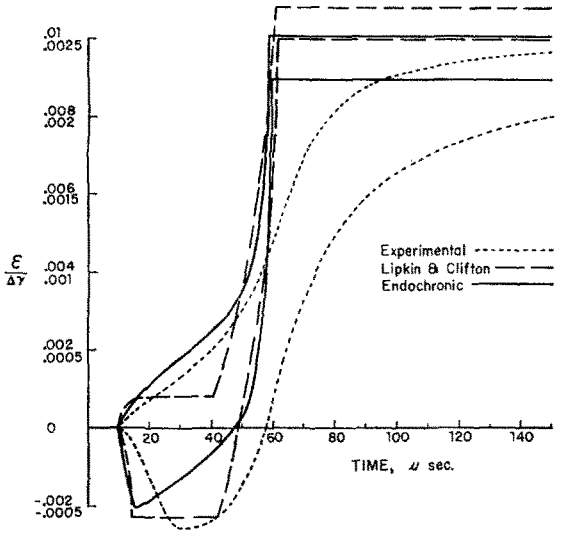

Fig. 5. Comparison of computed and experimental strain–time profiles at $x = 1{\cdot}875$ in. ($\tau_s = 3480$ psi, $u_0 = 500$ ips, $v_0 = 23$ ips).

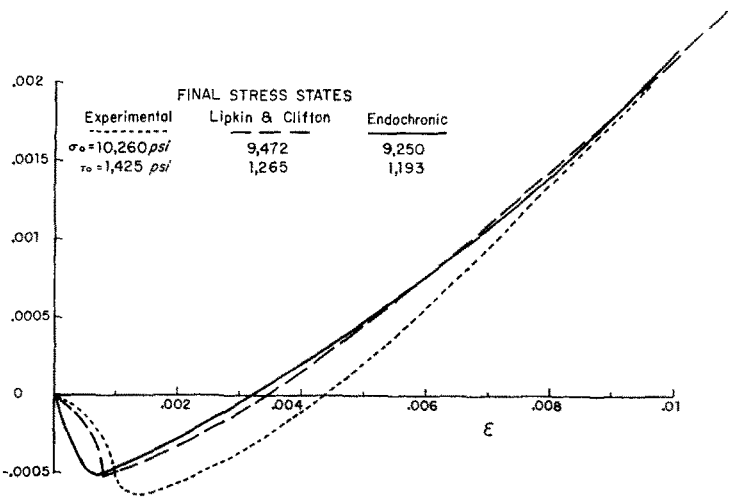

Fig. 6. Comparison of computed and experimental strain trajectories at $x = 1{\cdot}875$ in. ($\tau_s = 3480$ psi, $u_0 = 500$ ips, $v_0 = 23$ ips).

for the one-dimensional longitudinal case. Although the experimental results of Ref.[8] did not show this constant strain plateau, theoretically it should exist unless we take into account the effect of unloading behavior. The latter is evident, particularly, when the location x is very close to the tube end $x = 0$ such as the case shown in Fig. 5. As a consequence, the predicted final strains are always greater than the experimental results. In addition, we believe that the abrupt change from slow simple wave to the constant state region in the strain–time profiles is due to the negligence of the strain-rate dependence of materials. Further work is being done regarding the unloading behavior and the influence of the strain-rate on the dynamic behavior of materials.

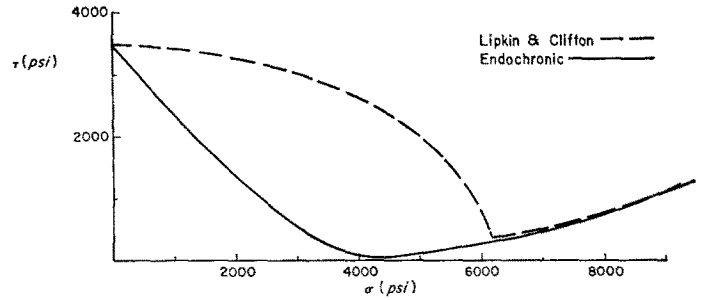

Fig. 7. Comparison of stress trajectories at $x = 1{\cdot}875$ in. ($\tau_s = 3480$ psi, $u_0 = 500$ ips, $v_0 = 23$ ips).

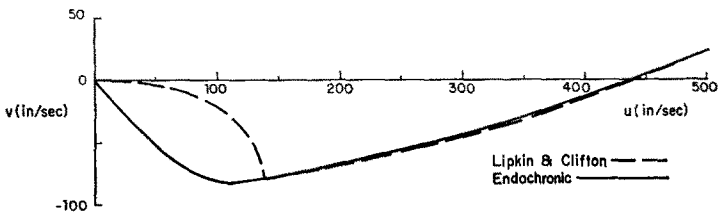

Fig. 8. Comparison of velocity trajectories at $x = 1{\cdot}875$ in. ($\tau_s = 3480$ psi, $u_0 = 500$ ips, $v_0 = 23$ ips).

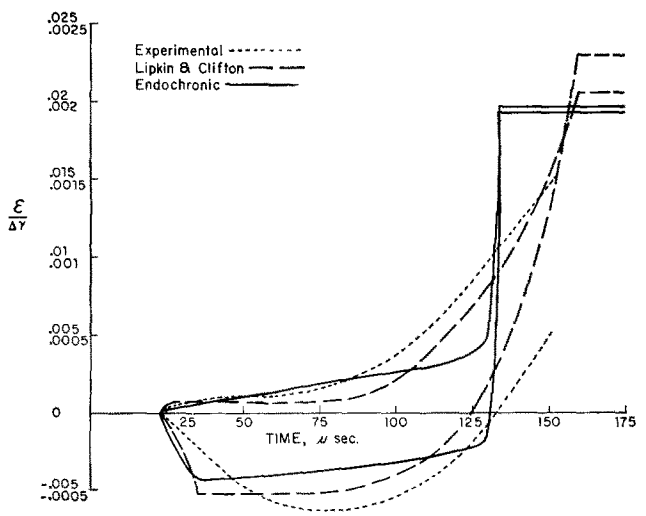

Fig. 9. Comparison of computed and experimental strain–time profiles at $x = 4{\cdot}5$ in. ($\tau_s = 2900$ psi, $u_0 = 800$ ips, $v_0 = 19$ ips).

The strain trajectory comparison reveals some differences among the theories and the experiment. As pointed out in Section 4, the directions of the strain-rate vector and the velocity vector are all coincident with the direction of the stress-rate vector. Accordingly, the differences in stress trajectory comparisons will carry over to the present comparison. Despite the aforementioned difference in fast wave region, the strain-trajectory in slow simple wave region agrees quite well with Lipkin and Clifton's results. Moreover, the final

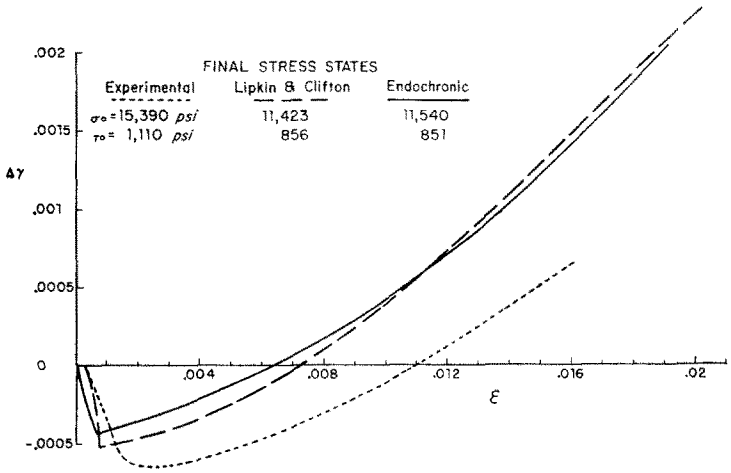

Fig. 10. Comparison of computed and experimental strain trajectories at $x = 4{\cdot}5$ in. ($\tau_s = 2900$ psi, $u_0 = 800$ ips, $v_0 = 19$ ips).

strain-states in the present theory are closer to the experimental values than those predicted by Lipkin and Clifton for all three examples presented here. The agreement between the present theory and Lipkin and Clifton's analysis is good in stress states at the boundary, but the agreement between the experimental and the theoretical boundary stresses is not good†. The discrepancy as explained in[8] may be due to the inaccuracy of the experimental value and the effect of strain-rate. In this analysis, the discrepancy may also be due to the inaccurate information regarding the shear stress–strain curve. Further experimental work needs to be done in getting the information for both longitudinal and torsional responses at the same time in order to explore the real material behavior along the complex loading paths.

The above numerical results have been obtained based on the assumption of material plastic incompressibility. No qualitative difference in results exist if the assumption of constant Poisson's ratio has been made. There is, however, a minor quantitative difference between the results of the two assumptions. In Fig. 3, we show the strain–time profiles based on both assumptions.

Acknowledgements—The authors wish to express their appreciation to Professors K. C. Valanis, R. J. Clifton and T. C. T. Ting for valuable discussions and comments.

REFERENCES

1. R. J. Clifton, An analysis of combined longitudinal and torsional plastic waves in a thin-walled tube, *Proc. 5th U. S. Nat. Congr. Appl. Mech.* Minnesota Univ. pp. 465–480 (1966).
2. J. Lipkin and R. J. Clifton, An experimental study of combined longitudinal and torsional plastic waves in a thin-walled tube, *Proc. 12th Int. Congr. Appl. Mech. Stanford Univ.*, pp. 292–304 (1968). Springer (1969).
3. R. P. Goel and L. E. Malvern, Biaxial plastic simple waves with combined kinematic and isotropic hardening, *J. Appl. Mech.*, **37**, 1100–1106 (Dec. 1970).
4. T. C. T. Ting, The initiation of combined stress waves in a thin-walled tube due to impact loading, *Int. J. Solids Struct.* **8**, 269–293 (1972).

† The authors are grateful to Prof. Clifton for providing the corrected experimental values on stresses.

5. T. C. T. Ting, Plastic wave propagation in linearly work-hardening materials, *J. appl. Mech.* (1974) to be published.
6. H. Fukuoka, Combined tension-torsion elastic–plastic waves as propagating singular surfaces, *Proc 20th Japan National Congr. Appl. Mech.* 231–235 (1970).
7. D. M. Janssen, S. K. Datta, and W. E. Jahsman, Propagation of weak waves in elastic–plastic solids, *J. Mech. Phys. Solids* **20**, 1–18 (1972).
8. J. Lipkin and R. J. Clifton, Plastic waves of combined stresses due to longitudinal impact of a pretorqued tube, Parts I and II, *J. Appl. Mech.* **37**, 1107–1120 (1970).
9. N. Cristescu, Dynamic plasticity under combined stress, *Symp. Mech. Behav. Mat. under Dynamic Loads, San Antonio*, pp. 329–342 (1967). Springer (1968).
10. K. C. Valanis, A theory of viscoplasticity without a yield surface, Part I and II, *Archiwum Mechaniki Stosowanej* **23**, 517–551 (1971).
11. H. J. Ivey, Plastic stress–strain relations and yield surfaces for aluminum alloys, *J. Mech. Eng. Sci.* **3**, 15–31 (1961).
12. A. Phillips and J. L. Tang, The effect of loading path on the yield surface at elevated temperatures *Int. J. Solids Struct.* **8**, 463–474 (1972).
13. T. Karman and P. Duwez, The propagation of plastic deformation in solids, *J. appl. Phys.* **21**, 987–994 (1950).
14. E. R. Wood and A. Phillips, On the theory of plastic wave propagation in a bar, *J. Mech. Phys. Solids* **15**, 241–254 (1967).
15. K. C. Valanis, Effect of prior deformation on cyclic response of metals, *J. appl. Mech.* (1974) to be published.

Абстракт — Теорию пластичности без поверхностного предела текучести применяют для получения разрешения распространения простой волны в тонкостенной трубе при комбинированной ступенчатой нагрузке. В настоящем анализе получили волны четырех скоростей распространения; все скорости включают комбинирование как продольных и торсиальных движений, так и поведение нагрузки и разгрузки. Представляем несколько численных примеров нашего теоретического анализа и сравнение их с экспериментальными данными и существующей теорией. В настоящем анализе не очевидна область постоянного состояния между медленными и быстрыми волнами. Это достаточно хорошо совпадает с опытом. Кроме того, предсказанное состояние относительного сдвига выше экспериментального, но ниже результатов, полученных Линкиным и Клифтоном.